

# **Sensitivity studies for searches for electroweak supersymmetry during run-II of the LHC**

by

Sesegma Sanzhieva

A thesis submitted in fulfilment  
of the requirements for the degree of  
Bachelor of Science  
in Maastricht University

## TABLE OF CONTENTS

<b>ABSTRACT</b> . . . . .	iii
<b>CHAPTERS</b>	
<b>I. Introduction</b> . . . . .	1
<b>II. Background information</b> . . . . .	3
2.1 The Standard Model . . . . .	3
2.1.1 The overview of the Standard Model . . . . .	3
2.1.2 Limitations of the SM . . . . .	4
2.2 Supersymmetry . . . . .	6
2.3 The ATLAS detector . . . . .	7
2.3.1 The ATLAS sub-detectors and trigger systems . . . . .	8
<b>III. Search for supersymmetry at the LHC</b> . . . . .	11
3.1 Introduction . . . . .	11
3.2 General search methods . . . . .	14
3.3 Overview of background processes . . . . .	16
3.4 Event selection and $b$ -tagging . . . . .	17
3.4.1 Event variables used in the analysis . . . . .	18
3.5 Cut-and-count approach and test statistics . . . . .	19
3.6 Computational tools . . . . .	20
<b>IV. Determining signal regions</b> . . . . .	21
4.1 First view . . . . .	21
4.2 Cuts in the SF channel . . . . .	22
<b>APPENDICES</b> . . . . .	24

## **ABSTRACT**

# CHAPTER I

## Introduction

High Energy Physics (HEP) is a branch of physics that studies elementary particles. The main way of studying physics experimentally at subatomic level is analysing information from particle collisions. Specific particles are accelerated to high speeds and directed to collide with each other producing an array of other particles that are then registered by detectors and studied by physicists. The largest currently functioning HEP experiment is the Large Hadron Collider (LHC) at CERN in Geneva, Switzerland. Since 2015, it is able to accelerate protons and create collisions at a centre-of-mass energy of 13 TeV. These collisions happen at two sites where the main particle detectors are situated. These experiments are ATLAS (A Toroidal LHC Apparatus) and CMS (Compact Muon Solenoid). Such high energy conditions of collisions emulate the state of the universe very shortly after the Big Bang and thus allow creation of particles that do not exist at normal conditions.

The underlying theory of modern HEP is the Standard Model (SM) and it has been very successful in describing subatomic particles and the interactions between them. It is a very robust theory that has been tested through a plethora of experiments at colliders. The most prominent success of previous LHC runs at 7 and 8 TeV centre-of-mass energy was the discovery of the Higgs particle, which was the final SM particle whose existence was proven experimentally [1, 2].

However, there are limitations to SM and there are a number of theories that try address these shortcomings. Collectively they are known as Beyond-the-Standard-Model (BSM) theories and present new theoretical frameworks aiming to explain physical world at a deeper level. One of the major BSM theories is supersymmetry (SUSY). It has a mathematically effective and elegant representation and, most importantly, overcomes some critical SM limitations.

Searches for evidence of supersymmetry are performed at the LHC along with other particle experiments. After runs at 7 and 8 TeV no significant evidence was

found and limits on masses of hypothetical supersymmetric particles have been placed. Higher energy collisions present a better chance of finding evidence of supersymmetry. The research presented in this thesis focuses on trying to design search methods in run-II (13 TeV) data that are sensitive to particular SUSY scenarios that feature electroweak production and decay. For that purpose a set of kinematic and topological variables are investigated as ways to determine presence of new particles.

## CHAPTER II

### Background information

#### 2.1 The Standard Model

##### 2.1.1 The overview of the Standard Model

The underlying theory of modern High Energy Physics is the Standard Model (SM). This theory has been developed in the second half of the 20th century with contributions from many scientists and it is a very successful representation of the world on the subatomic level. The SM classifies all known subatomic particles into specific categories and provides the description of the interactions between them.

In the SM there are two main types of fermions (1/2-spin particles) known as quarks and leptons. Each family has three generations with each consecutive generation being heavier than the previous. The up and down quarks along with the electron are stable and constitute ordinary matter. The interactions between fermions are mediated through the exchange of force carrier particles known as gauge bosons (see Tab. 2.1). The final piece in the SM is the Higgs boson and it gives mass to other fundamental particles. All bosons possess integer spin [3]. Further nomenclature identifies hadrons - composite particles that are made of quarks and gluons.

The mathematical representation of the SM is built within the broader frame of Group Theory. Employing the official terminology, the SM has the symmetry group

Fermion	Generations			Bosons
Leptons	$e$	$\mu$	$\tau$	$Z$
	$\nu_e$	$\nu_\mu$	$\nu_\tau$	$W^\pm$
Quarks	$u$	$c$	$t$	photon
	$d$	$s$	$b$	gluon

Table 2.1: The Standard Model particles

$U(1)_Y \times SU(2)_L \times SU(3)$ . The  $SU(3)$  symmetry group generates strong interactions, that describe processes involving quarks and gluons. These processes are described by the theory of Quantum Chromodynamics and the particles possess a specific type of charge known as “colour charge”. The  $U(1)_Y \times SU(2)_L$  group generates electroweak interactions. At energies below 100 GeV, however, the single electroweak interaction is broken into the weak and electromagnetic varieties with the symmetry group  $U(1)_{\text{em}}$ . The unification of these two types was the result of efforts by Glashow, Weinberg and Salam [4, 5, 6]. The weak interaction processes involve fermions and are mediated by electrically charged  $W^\pm$  bosons for charged processes and the chargeless  $Z$  gauge boson for neutral ones. Finally, the electromagnetic force is mediated by photons and only involves electrically charged particles.

Above the unification energy of 100 GeV, and thus before the spontaneous electroweak symmetry breaking through Higgs mechanism [7, 8], the gauge bosons are different. There are three  $W$  bosons, denoted  $W^1$ ,  $W^2$ ,  $W^3$  corresponding to the  $SU(2)_L$  part of the group and one  $B$  boson corresponding to the  $U(1)_Y$  part. All the electroweak bosons are massless, and acquire mass by coupling to the Higgs field in the process of symmetry breaking.

### 2.1.2 Limitations of the SM

The predictions of the SM have been successfully tested in particle accelerator experiments, and its final confirmation came with the discovery of the Higgs boson in 2012 - a true scientific breakthrough. This was the last missing piece of experimental evidence needed for the full validation of the SM. The experiments that led to this discovery were conducted at CERNs Large Hadron Collider (LHC) in run-I proton-proton collisions at centre-of-mass energy  $\sqrt{s} = 7$  and the later upgrade to 8 TeV. Despite the fact that the SM has proven to be an extremely precise and successful theory there are some caveats for which it does not provide adequate solutions.

One of the inconsistencies within the SM is the so-called Hierarchy problem [9]. One of the ways it reveals itself is through the large discrepancy between the Planck mass and the mass of the Higgs particle. The former is about  $10^{17}$  times bigger than the latter and current representation of particle physics cannot explain such a big difference. Quantum effects start manifesting themselves at the Plank mass threshold and such a vast difference between these two values is yet unaccounted for.

Another prominent problem is that the SM does not explain dark matter. While ordinary matter only constitutes about 5% in the total mass-energy content of the universe, it is dark matter and dark energy that account for the rest [10]. The SM

does not provide a candidate particle for dark matter and thus is only able to describe ordinary matter and energy.

One of the main challenges of modern physics is the unification of forces. This is part of the ongoing attempts to reach the ultimate goal - a “theory of everything”. Such a theory would have to account for all physical aspects of the universe and include the most fundamental structures and interactions. The first step was made with the unification of electromagnetic and weak forces. The next step is to achieve the unification of electromagnetic, weak, and strong interaction forces this step is the Grand Unification. The ultimate step is to combine all four fundamental forces together, which means adding gravity, in what is called Super Unification (see Fig. 2.1). Thus far quantum field theory and general relativity are able to describe phenomena on their respective scale of action with remarkable precision, but are fundamentally incompatible.

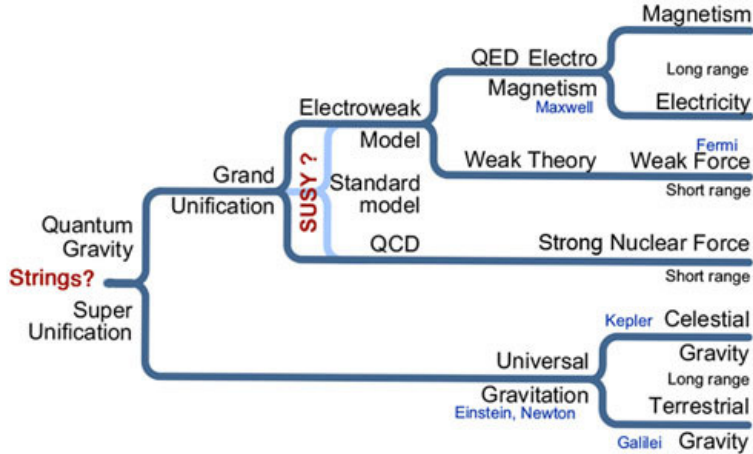


Figure 2.1: Various stages in the unification of forces [11]

Within the confines of the SM even the Grand Unification is not possible, and this prompts the search for new theories that account for this and other shortcomings of the SM. Collectively they are called Beyond-Standard-Model (BSM) theories. Among these, there are theories that include extra-dimensions, composite Higgs boson models, etc. Theoretical and experimental search for BSM physics is the current frontier of HEP and one of the most important questions in science overall.

## 2.2 Supersymmetry

One of the strongest candidate framework theories that can offer solutions to the SM deficiencies is supersymmetry (SUSY) [12]. SUSY is a spacetime symmetry that equates fermionic and bosonic degrees of freedom. Among several theories that are based on SUSY principles, the Minimal Supersymmetric Standard Model (MSSM) offers the simplest extention of the SM. The MSSM postulates that each SM particle has a supersymmetric partner which is different only in spin by one-half unit while all other quantum numbers stay the same. The superpartners of quarks, leptons, and neutrinos are called squarks, sleptons and sneutrinos. For gauge bosons the superpartners are gluinos, photino, winos and binos, collectively named gauginos. The latter two are superpartners of the B and three W bosons of the elecrownreak interaction before electroweak symmetry breaking. It follows naturally since SUSY is invoked before the electroweak symmetry breaking. The Higgs sector in SUSY has five superpartners - two charged ( $H^\pm$ ) particles and three neutral ones ( $h^0, H^0, A^0$ ). They are known collectively as Higgsinos. Mixing between winos, binos and Higgsinos results in charginos and neutralinos. Their mass eigenstates are referred to as  $\tilde{\chi}_i^\pm$  ( $i = 1,2$ ) and  $\tilde{\chi}_i^0$  ( $i = 1,2,3,4$ ) in order fo increasing mass.

The MSSM belongs to a class of theories that all share the same requirement - a quantity known as R-parity has to be conserved in interactions. The mathematical description of R-parity is beyond the scope of this paper. However, one important consequence of R-parity conservation is that if supersymmetric particles were to be produced in collisions, they would be created in pairs. Then they decay through various possible scenarios with the lightest supersymmetric particle (LSP) emerging in the final state and escaping undetected. Because the LSP is stable it provides a possible candidate for the dark matter particle.

The MSSM imposes 105 free parameters and this is one of its major issues, since any analysis will be addled with enormous complexity stemming from high dimensionality. There are various simplified models that reduce the number of free parameters to manageable values through various theoretically and experimentally motivated constraints. One of them is the phenomenological Minimal Supersymmetric Standard Model (pMSSM) that contains only 19 free parameters and which will be used in this thesis' analysis.

## 2.3 The ATLAS detector

The ATLAS experiment is a multi-purpose particle detector with cylindrical geometry and has a nominal forward-backward symmetry [13]. The dimensions of the detector are 25 m in height and 44 m in length and the overall weight of the detector is approximately 7000 tonnes. It can detect particles with almost  $4\pi$  coverage in solid angle around the collision point, which covers almost all of the spherical area around the center.

Proton bunches are accelerated in the underground ring that is 27 km in diameter and are directed to collide inside the detectors. The collisions happen at 40 MHz bunch crossing rate, with an average 23 interactions per bunch crossing. The LHC is designed to operate at  $\sqrt{s}=14$  TeV and instantaneous luminosity  $\mathcal{L} = 10^{34}$  cm $^{-2}$  s $^{-1}$  in proton-proton collision mode. Instantaneous luminosity is defined as follows

$$\mathcal{L} = \frac{1}{\sigma} \frac{dN}{dt} \quad (2.1)$$

Where  $\sigma$  is the interaction cross-section, and  $N$  is the number of detected events during time  $t$ . Integrated luminosity  $\int \mathcal{L} dt$  is a quantity that expresses the amount of total data gathered during the time  $t$  of running the LHC. Luminosity is particularly useful as a way to express the amount of data gathered, because it allows to find number of events for a particular process simply by multiplying this process's cross-section by the value of luminosity. The analysis presented in this paper uses the dataset recorded at 3.2 fb $^{-1}$  of integrated luminosity throughout run-II of the LHC during 2015.

The Cartesian coordinate system used at ATLAS has its origin at the nominal point of interaction with the  $z$  axis extending along the particle beam longitudinally, the positive  $x$  axis pointing towards the center of the ring, and the positive  $y$  axis pointing upwards. The geometry of the detector makes the use of cylindrical coordinate system especially convenient. Using it, the  $z$  axis stays the same, the polar angle  $\theta$  is the angle from the  $z$ -axis, and the azimuthal angle  $\phi$  encircles the  $z$  axis in the transverse plane. However, instead of  $\theta$  it is more convenient to use pseudorapidity  $\eta$ , due to the fact that differences in pseudorapidity are close to invariant under Lorentz boosts along the  $z$  axis (fully invariant for real rapidity).  $\eta$  is defined as follows

$$\eta = -\ln\left(\tan \frac{\theta}{2}\right) \quad (2.2)$$

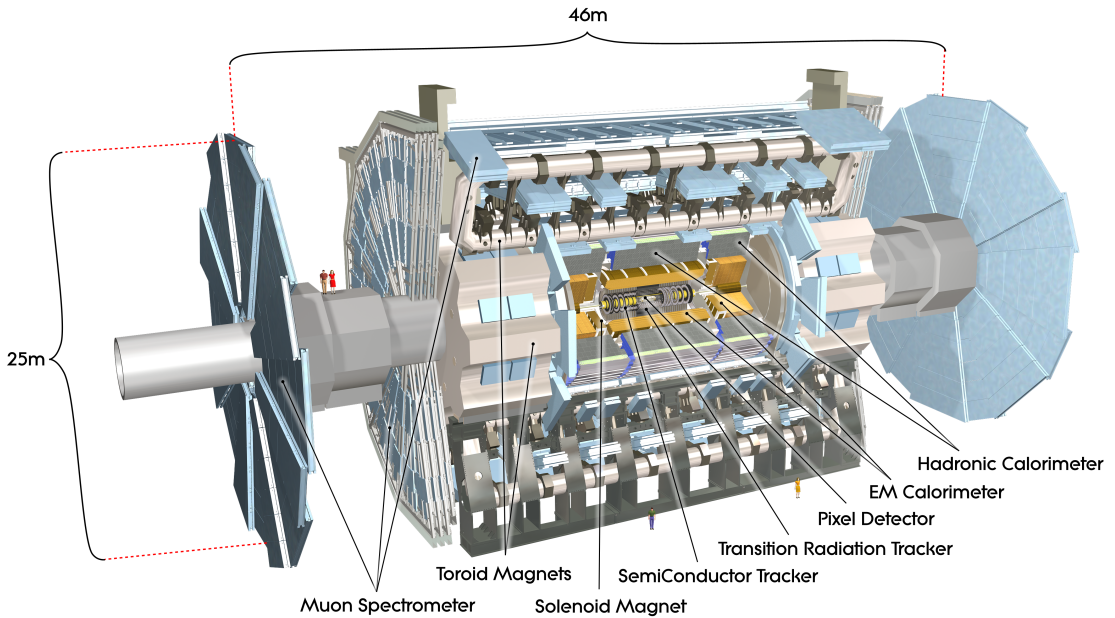


Figure 2.2: Cut-away view of the ATLAS detector (people are included for scale comparison) [13].

### 2.3.1 The ATLAS sub-detectors and trigger systems

The ATLAS detector consists of several subdetector layers with each layer performing a specific function (see Fig. 2.3). The Inner Detector (ID) performs tracking of newly created particles. It is closest to the collision point and covers  $|\eta| < 2.5$  in pseudorapidity. The ID has high granularity as it is exposed to the highest density of particle interaction. It was designed to provide a transverse momentum resolution and a transverse impact parameter resolution [14]. The detector itself consists of three separate subsystems. The main components of the ID are the silicon pixel detector, the semiconductor tracker, and the transition radiation tracker. Ahead of the run-II a new pixel layer, called the Insertable B-Layer (IBL), has been added to the ID improving the resolution and particle identification qualities. All these layers are immersed in a 2 T magnetic field, created by the thin superconducting solenoidal magnet. This field is parallel to the beam axis and bends trajectories of charged particles allowing their charge and momentum identification based on the characteristic bending of their trajectories.

The next two layers are the two calorimeters that measure energies of specific types of particles. The particles travel through the detectors and lose their energy via

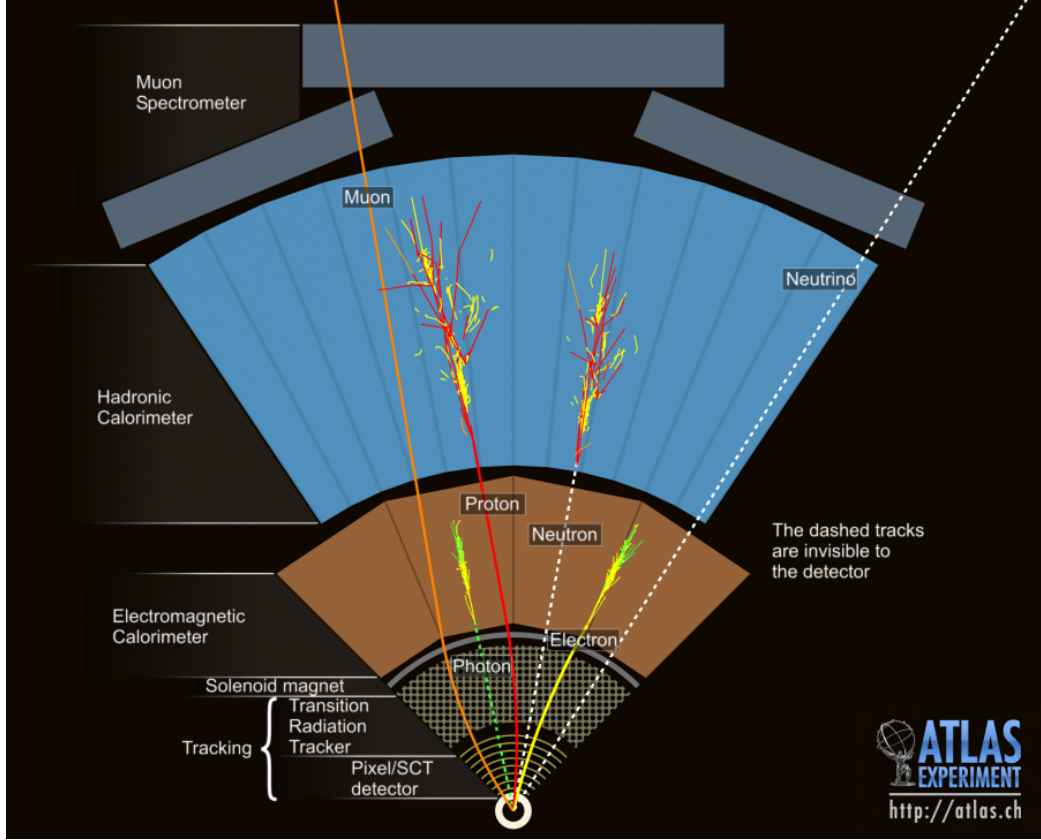


Figure 2.3: Event in the transverse plane, a computer generated image of the ATLAS detector [15].

interaction with its layers leaving energy deposits as they move through the material. The first one is the high-granularity Electromagnetic Calorimeter (EmCal) and it measures energies of electrons and photons. Coloured particles (gluons and quarks) form “jets” that travel further into Hadronic calorimeter (HCal) where they continue their decays and also deposit their available energy. Both calorimeters are designed to provide good quality measurements of momentum and energy and cover the region  $|\eta| < 4.9$ .

The final detecting layer is the Muon spectrometer (MS), which tracks and measures charged particles, specifically muons. Muons do not interact with matter as strongly as electrons so they travel further without radiating much energy in the calorimeters. The MS is immersed into a large toroidal magnet, that provides a magnetic field throughout the spectrometer and bends the trajectories of charged muons, which makes it possible to detect their charge and momentum. Any particles that are not covered by the described sub-detectors will escape undetected. These include neutrinos and, possibly, the LSP.

Triggers are used to select events by identifying signatures of various particles as well as using global event signatures, such as missing transverse energy [16]. A multilevel trigger system is used at ATLAS to select events that are of interest to further offline analysis. The first level is hardware-based and uses information from the calorimeters and muon spectrometer, the second and third levels are software-based and use information from all sub-detectors. Because the data at the LHC is produced in staggering amounts employing efficient trigger systems is crucial to be able to extract information that is relevant for further analysis. At  $\sqrt{s}=13$  TeV the spacing between bunches crossing is 25 ns and the collision rate is 40 MHz. This rate has to be reduced to  $O(500$  Hz) to be able to keep data in permanent memory devices [17].

Ideally, a trigger should be able to retain a maximum number of events that are interesting for physics analysis and reject as many background events as possible. In this regard the concept of trigger efficiency is very important, and this efficiency varies depending on the particular process that is being investigated. The overall goal is to reduce data from the raw amount to the size at which it can be stored permanently and at the same time keeping as many relevant events as possible.

## CHAPTER III

# Search for supersymmetry at the LHC

### 3.1 Introduction

Searches for various BSM theories including SUSY have been performed at the LHC alongside searching for the Higgs and performing different SM analyses. Many SUSY searches were conducted targeting the production of squarks and gluinos. This was motivated by a larger theoretical cross-section and therefore higher probability of producing coloured superpartners [18]. Up to this moment no statistically significant excess over the SM has been detected and exclusion limits were placed on masses of SUSY particles. Figure 3.1 shows the latest data on the masses that have been excluded for supersymmetric particles in various production scenarios. The lower limits on the masses of most squarks and gluinos in different searches significantly exceed 1 TeV [19]. As a consequence, if their production occurs, it is either extremely rare at present energies or requires higher energy of collision to leave an identifiable signature.

This thesis's research will focus on the electroweak production as one of the possible SUSY particle production scenarios. Sleptons and gauginos are produced in electroweak production processes and are not affected by the strong force. They have smaller cross-sections compared to squarks and gluinos, so their theoretical production rate is smaller. However, if their masses are small compared to the strongly interacting sparticles, SUSY production will likely be dominated by electroweak production where sparticles have smaller mass and current energy might be enough to produce them in quantities that would allow their detection [20].

## ATLAS SUSY Searches\* - 95% CL Lower Limits

Status: March 2016

ATLAS Preliminary

$\sqrt{s} = 7, 8, 13 \text{ TeV}$

Model	$e, \mu, \tau, \gamma$	Jets	$E_T^{\text{miss}}$	$\int L dt [\text{fb}^{-1}]$	Mass limit	$\sqrt{s} = 7, 8 \text{ TeV}$	$\sqrt{s} = 13 \text{ TeV}$	Reference
MSUGRA/CMSSM	0-3 $e, \mu, 1/2 \tau$	2-10 jets + 3 $b$	Yes	20.3	$\tilde{q}, \tilde{\bar{q}}$	980 GeV	1.85 TeV	1507.05625
$\tilde{q}\tilde{q}, \tilde{q}\tilde{q} \rightarrow q\tilde{q}^0_1$ (compressed)	mono-jet 2 $e, \mu$ (off-Z)	6 jets	Yes	3.2	$\tilde{q}$	610 GeV	1.4 TeV	ATLAS-CONF-2015-062 <i>To appear</i>
$\tilde{q}\tilde{q}, \tilde{q}\tilde{q} \rightarrow q\tilde{q}^0_1 (l\nu) \nu \chi^0_1$	0	2 jets	Yes	20.3	$\tilde{q}$	820 GeV	1.52 TeV	1503.03290
$\tilde{g}\tilde{g}, \tilde{g}\tilde{g} \rightarrow gg\chi^0_1 \rightarrow ggW^+ \chi^0_1$	1-6 jets	Yes	3.2	$\tilde{g}$	-	1.6 TeV	1.38 TeV	ATLAS-CONF-2015-062
$\tilde{g}\tilde{g}, \tilde{g}\tilde{g} \rightarrow gg\chi^0_1 \rightarrow gg(l/\ell^+/\ell^-) \chi^0_1$	2 $e, \mu$	3-6 jets	Yes	3.3	$\tilde{g}$	-	1.52 TeV	ATLAS-CONF-2015-076
$\tilde{g}\tilde{g}, \tilde{g}\tilde{g} \rightarrow gg\chi^0_1 \rightarrow gg(l/\ell^+/\ell^-) \chi^0_1$	2 $e, \mu$	0-3 jets	-	20	$\tilde{g}$	-	1.38 TeV	1501.03555
$\tilde{g}\tilde{g}, \tilde{g}\tilde{g} \rightarrow gg\chi^0_1 \rightarrow gg(l/\ell^+/\ell^-) \chi^0_1$	0	7-10 jets	Yes	3.2	$\tilde{g}$	-	1.4 TeV	1602.06194
GMSB ( $\tilde{l}$ NLSP)	1-2 $\tau + 0.1 \ell$	0-2 jets	Yes	20.3	$\tilde{l}$	-	1.63 TeV	1407.06033
GGM (higgsino-bino NLSP)	2 $\gamma$	-	Yes	20.3	$\tilde{l}$	-	1.34 TeV	1507.05493
GGM (higgsino-bino NLSP)	$\gamma$	1 jet	Yes	20.3	$\tilde{l}$	-	1.37 TeV	1507.05493
GGM (higgsino NLSP)	2 $e, \mu / Z$	2 jets	Yes	20.3	$\tilde{l}$	-	1.3 TeV	1503.03290
Gravitino LSP	0	mono-jet	Yes	20.3	$\tilde{l}$	-	900 GeV	1502.01518
$\tilde{g}, \tilde{g} \rightarrow h\tilde{b}^0_1$	0-1 $e, \mu$	3 jets	Yes	3.3	$\tilde{g}$	-	1.76 TeV	ATLAS-CONF-2015-067
$\tilde{g}, \tilde{g} \rightarrow h\tilde{b}^0_1$	0-1 $e, \mu$	3 jets	Yes	20.1	$\tilde{g}$	-	1.78 TeV	<i>To appear</i>
$\tilde{g}, \tilde{g} \rightarrow h\tilde{b}^0_1$	0	3 jets	Yes	3.3	$\tilde{g}$	-	1.76 TeV	1407.06000
$\tilde{g}, \tilde{g} \rightarrow h\tilde{b}^0_1$	0	3 jets	Yes	20.1	$\tilde{g}$	-	1.37 TeV	1506.08616
Inclusive Searches	gen	gen	gen	3.2	$\tilde{b}_1, \tilde{b}_1, \tilde{b}_1 \rightarrow b\tilde{b}^0_1$	840 GeV	840 GeV	ATLAS-CONF-2015-066
Inclusive Searches	gen	gen	gen	3.2	$\tilde{b}_1, \tilde{b}_1, \tilde{b}_1 \rightarrow b\tilde{b}^0_1$	325-540 GeV	325-540 GeV	1602.09058
Inclusive Searches	gen	gen	gen	3.2	$\tilde{b}_1, \tilde{b}_1, \tilde{b}_1 \rightarrow b\tilde{b}^0_1$	200-500 GeV	200-500 GeV	1209.2102, 1407.0563
Inclusive Searches	gen	gen	gen	3.2	$\tilde{b}_1, \tilde{b}_1, \tilde{b}_1 \rightarrow b\tilde{b}^0_1$	90-198 GeV	90-198 GeV	1506.08616, 1506.08617
Inclusive Searches	gen	gen	gen	3.2	$\tilde{b}_1, \tilde{b}_1, \tilde{b}_1 \rightarrow b\tilde{b}^0_1$	205-715 GeV	205-715 GeV	ATLAS-CONF-2016-007
Inclusive Searches	gen	gen	gen	3.2	$\tilde{b}_1, \tilde{b}_1, \tilde{b}_1 \rightarrow b\tilde{b}^0_1$	745-785 GeV	745-785 GeV	1407.0608
Inclusive Searches	gen	gen	gen	3.2	$\tilde{b}_1, \tilde{b}_1, \tilde{b}_1 \rightarrow b\tilde{b}^0_1$	-	-	1403.5222
Inclusive Searches	gen	gen	gen	3.2	$\tilde{b}_1, \tilde{b}_1, \tilde{b}_1 \rightarrow b\tilde{b}^0_1$	-	-	1506.08616
EW direct	gen, squarks	gen, squarks	gen, squarks	3.2	$\tilde{b}_1, \tilde{b}_1, \tilde{b}_1 \rightarrow b\tilde{b}^0_1$	-	-	1403.5294
EW direct	gen	gen	gen	3.2	$\tilde{b}_1, \tilde{b}_1, \tilde{b}_1 \rightarrow b\tilde{b}^0_1$	-	-	1403.5294
EW direct	gen	gen	gen	3.2	$\tilde{b}_1, \tilde{b}_1, \tilde{b}_1 \rightarrow b\tilde{b}^0_1$	-	-	1407.0350
EW direct	gen	gen	gen	3.2	$\tilde{b}_1, \tilde{b}_1, \tilde{b}_1 \rightarrow b\tilde{b}^0_1$	-	-	1402.7029
EW direct	gen	gen	gen	3.2	$\tilde{b}_1, \tilde{b}_1, \tilde{b}_1 \rightarrow b\tilde{b}^0_1$	-	-	1403.5294, 1402.7029
EW direct	gen	gen	gen	3.2	$\tilde{b}_1, \tilde{b}_1, \tilde{b}_1 \rightarrow b\tilde{b}^0_1$	-	-	1501.07110
EW direct	gen	gen	gen	3.2	$\tilde{b}_1, \tilde{b}_1, \tilde{b}_1 \rightarrow b\tilde{b}^0_1$	-	-	1405.5086
EW direct	gen	gen	gen	3.2	$\tilde{b}_1, \tilde{b}_1, \tilde{b}_1 \rightarrow b\tilde{b}^0_1$	-	-	1507.05493
Long-lived particles	Direct $\tilde{l}^+ \tilde{l}^-$ prod., long-lived $\tilde{\chi}^\pm_1$	2 $e, \mu$	0	Yes	$\tilde{l}$	90-335 GeV	90-335 GeV	1403.5294
Long-lived particles	Direct $\tilde{l}^+ \tilde{l}^-$ prod., long-lived $\tilde{\chi}^\pm_1$	2 $e, \mu$	0	Yes	$\tilde{l}$	140-475 GeV	140-475 GeV	1403.5294
Long-lived particles	Direct $\tilde{l}^+ \tilde{l}^-$ prod., long-lived $\tilde{\chi}^\pm_1$	2 $e, \mu$	0	Yes	$\tilde{l}$	355 GeV	355 GeV	1407.0350
Long-lived particles	Direct $\tilde{l}^+ \tilde{l}^-$ prod., long-lived $\tilde{\chi}^\pm_1$	3 $e, \mu$	0	Yes	$\tilde{l}$	715 GeV	715 GeV	1402.7029
Long-lived particles	Direct $\tilde{l}^+ \tilde{l}^-$ prod., long-lived $\tilde{\chi}^\pm_1$	3 $e, \mu$	0-2 jets	Yes	$\tilde{l}$	425 GeV	425 GeV	1403.5294, 1402.7029
Long-lived particles	Direct $\tilde{l}^+ \tilde{l}^-$ prod., long-lived $\tilde{\chi}^\pm_1$	3 $e, \mu$	0-2 jets	Yes	$\tilde{l}$	270 GeV	270 GeV	1501.07110
Long-lived particles	Direct $\tilde{l}^+ \tilde{l}^-$ prod., long-lived $\tilde{\chi}^\pm_1$	4 $e, \mu$	0	Yes	$\tilde{l}$	635 GeV	635 GeV	1405.5086
Long-lived particles	Direct $\tilde{l}^+ \tilde{l}^-$ prod., long-lived $\tilde{\chi}^\pm_1$	1 $e, \mu$	+	Yes	$\tilde{l}$	115-370 GeV	115-370 GeV	1507.05493
Long-lived particles	Disapp. trk	1 jet	Yes	20.3	$\tilde{\chi}^\pm_1$	270 GeV	270 GeV	1310.3675
Long-lived particles	Disapp. trk	1 jet	Yes	18.4	$\tilde{\chi}^\pm_1$	495 GeV	495 GeV	1506.05332
Long-lived particles	Disapp. trk	1 jet	Yes	27.9	$\tilde{\chi}^\pm_1$	850 GeV	850 GeV	1310.6584
Long-lived particles	Disapp. trk	1 jet	-	3.2	$\tilde{\chi}^\pm_1$	-	-	<i>To appear</i>
Long-lived particles	Stable $\tilde{e}, \tilde{\chi}^0_1 \rightarrow \tilde{e}, \tilde{\chi}^0_1$	1-2 $\mu$	-	-	$\tilde{\chi}^0_1$	537 GeV	537 GeV	1411.6795
Long-lived particles	Stable $\tilde{e}, \tilde{\chi}^0_1 \rightarrow \tilde{e}, \tilde{\chi}^0_1$	1-2 $\mu$	-	-	$\tilde{\chi}^0_1$	440 GeV	440 GeV	1409.55162
Long-lived particles	Stable $\tilde{e}, \tilde{\chi}^0_1 \rightarrow \tilde{e}, \tilde{\chi}^0_1$	1-2 $\mu$	-	-	$\tilde{\chi}^0_1$	1.0 TeV	1.0 TeV	1504.05162
Long-lived particles	Stable $\tilde{e}, \tilde{\chi}^0_1 \rightarrow \tilde{e}, \tilde{\chi}^0_1$	1-2 $\mu$	-	-	$\tilde{\chi}^0_1$	1.0 TeV	1.0 TeV	1503.04430
RPV	$pp \rightarrow \nu_l \bar{\nu}_l + e \bar{\nu}_l / \mu \bar{\nu}_l / \tau \bar{\nu}_l$	$e \bar{e}, \mu \bar{\nu}_l, \tau \bar{\nu}_l$	-	-	$\tilde{\nu}_l$	1.7 TeV	1.7 TeV	1404.2500
RPV	$pp \rightarrow \nu_l \bar{\nu}_l + e \bar{\nu}_l / \mu \bar{\nu}_l / \tau \bar{\nu}_l$	$e \bar{e}, \mu \bar{\nu}_l, \tau \bar{\nu}_l$	-	-	$\tilde{\nu}_l$	1.45 TeV	1.45 TeV	1405.5086
RPV	$pp \rightarrow \nu_l \bar{\nu}_l + e \bar{\nu}_l / \mu \bar{\nu}_l / \tau \bar{\nu}_l$	$e \bar{e}, \mu \bar{\nu}_l, \tau \bar{\nu}_l$	-	-	$\tilde{\nu}_l$	760 GeV	760 GeV	1405.5086
RPV	$pp \rightarrow \nu_l \bar{\nu}_l + e \bar{\nu}_l / \mu \bar{\nu}_l / \tau \bar{\nu}_l$	$e \bar{e}, \mu \bar{\nu}_l, \tau \bar{\nu}_l$	-	-	$\tilde{\nu}_l$	450 GeV	450 GeV	1502.05686
RPV	$pp \rightarrow \nu_l \bar{\nu}_l + e \bar{\nu}_l / \mu \bar{\nu}_l / \tau \bar{\nu}_l$	$e \bar{e}, \mu \bar{\nu}_l, \tau \bar{\nu}_l$	-	-	$\tilde{\nu}_l$	917 GeV	917 GeV	1502.05686
RPV	$pp \rightarrow \nu_l \bar{\nu}_l + e \bar{\nu}_l / \mu \bar{\nu}_l / \tau \bar{\nu}_l$	$e \bar{e}, \mu \bar{\nu}_l, \tau \bar{\nu}_l$	-	-	$\tilde{\nu}_l$	980 GeV	980 GeV	1404.2500
Other	Scalar charm, $\tilde{c} \rightarrow c \tilde{\chi}^0_1$	0	2 $e, \mu$	2 jets + 2 $b$	-	320 GeV	320 GeV	1601.07453
Other	Scalar charm, $\tilde{c} \rightarrow c \tilde{\chi}^0_1$	0	2 $e, \mu$	2 jets + 2 $b$	-	510 GeV	510 GeV	1501.01325

\*Only a selection of the available mass limits on new states or phenomena is shown.

Figure 3.1: Exclusion limits of ATLAS searches for supersymmetry. Squark and gluon masses are predominantly above the 1 TeV. [21]

So far searches in the electroweak region have been unable to find evidence of supersymmetric particles. Limits on their masses according to various decay scenarios have been obtained and can be seen in Fig 3.2.

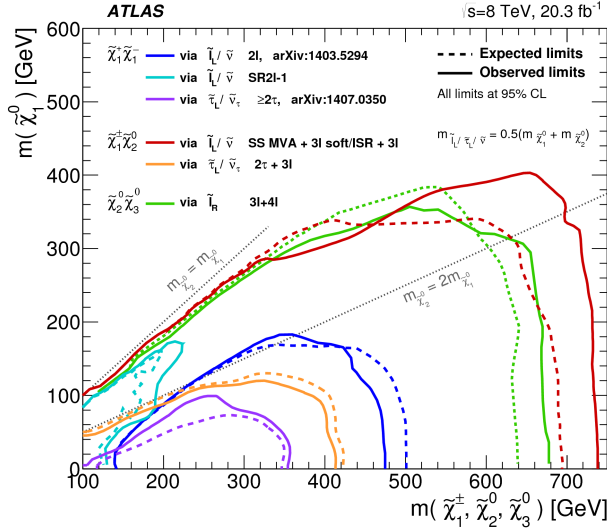


Figure 3.2: The 95% CL exclusion limits on  $\tilde{\chi}_1^+ \tilde{\chi}_1^-$ ,  $\tilde{\chi}_1^\pm \tilde{\chi}_2^0$  and  $\tilde{\chi}_2^0 \tilde{\chi}_3^0$  production with  $\tilde{\ell}$ -mediated decays, as a function of the  $\tilde{\chi}_1^\pm$ ,  $\tilde{\chi}_2^0$  and  $\tilde{\chi}_3^0$  masses [22].

These results are taken from the analysis performed at  $\sqrt{s} = 8$  TeV and integrated luminosity of  $20.3 \text{ fb}^{-1}$  [20]. The search was performed based on various scenarios of the MSSM, involving electroweak production of charginos and neutralinos. The turquoise and blue lines represent decay scenarios that are relevant for this paper as they show information on slepton-mediated decays of a chargino pair. In particular, the production of a  $\tilde{\chi}_1^+ \tilde{\chi}_1^-$  pair decaying through a slepton ( $\tilde{\ell}$ ) with final states containing two opposite sign leptons will be considered (see Fig. 3.3).

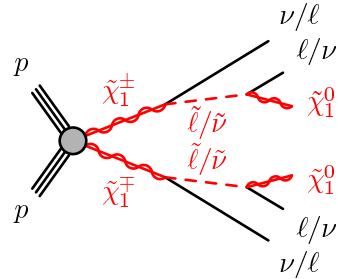


Figure 3.3: Electroweak chargino pair production in proton-proton collisions with intermediate slepton in the decay process.

In this thesis three different patterns of mass-splitting between the chargino and

the neutralino will be considered. Denoted by the pair of numbers assigned to the masses (in GeV) of the chargino and the neutralino respectively, they are 600-100, 400-200, and 200-150 signal models. The choice for these signals is motivated by the fact that they are not covered by the exclusion limits shown in Fig. 3.3 and their variety in terms of mass splitting. For all of them the mass of the intermediate slepton is set to be  $m_{\tilde{\ell}} = 0.5(m_{\tilde{\chi}_1^\pm} + m_{\tilde{\chi}_1^0})$ .

The cross-section of the investigated production process depends on the mass of the chargino - lighter ones are more likely to be produced and therefore have a larger cross-sections. Fig. 3.4 shows the distribution of the theoretical cross sections depending on the mass of the chargino. The cross sections for this process were obtained from [23, 24].

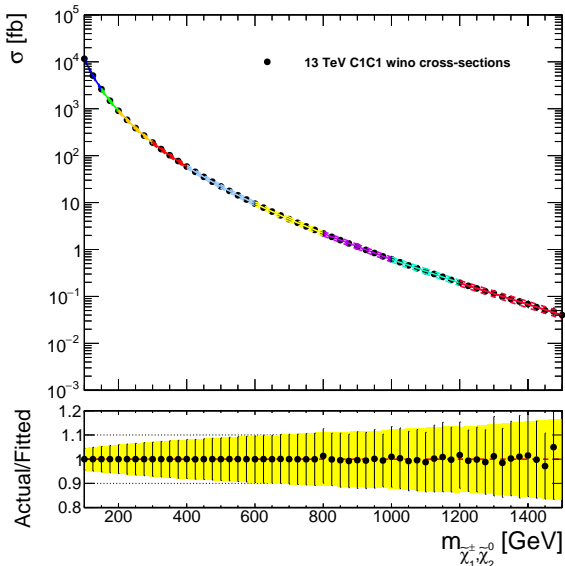


Figure 3.4: The distribution of cross-sections for slepton-mediated chargino decay [25].

In the nomenclature used at LHC and in this thesis, electrons and muons are called “light leptons”. Taus are considered separately as they decay very promptly and therefore are very difficult to reconstruct. This thesis only focuses on final states containing electrons and muons and thus the designation “lepton” only refers to these particles.

### 3.2 General search methods

Detecting new physics events at LHC requires using computational and statistical methods that can deal with the type of information a particle accelerator produces.

The data is initially collected using triggers corresponding to the type of events under analysis. Each event has a large number of physical characteristics such as momentum, energy, mass, multiplicities, etc. The numbers representing them are all stored in a data structure which then can be accessed, modified and analysed using software tools.

The cornerstone of all accelerator physics analyses is the correct estimation of background events. All background events represent physics that is already known and that has some similar or identical features with the processes under investigation. For instance, this thesis focusses on the reactions that have precisely two oppositely charged leptons in their final states. A number of processes well described by the standard model share this characteristic and therefore will form the background.

The task of correctly identifying background is therefore crucial in the process of searches for new physics events. Monte Carlo (MC) simulations are used to generate background events distribution samples according to a probability density function of a particular process. In this thesis MC simulated data samples are used to model SM background events along with SUSY signal events. All the samples include events that can result in dileptonic decays.

The data is then overlaid on the simulated background to see whether there is a disagreement between data and background. If there is a significantly large excess of data over background it can lead to new discoveries such as the existence of a new particle. The presence of a new particle can reveal itself in a number of ways. The straightforward way to detect a new physics event is an abnormality in some distribution of the data, as was the case with the discovery of the Higgs (see Fig. 3.5). The narrow peak over a smooth line in mass distribution of diphoton events constituted a significant excess over the SM predictions and was in agreement with theoretical predictions [1].

Unfortunately, this method does not work well for SUSY particles and other techniques have to be used. Standard search techniques involve defining **signal regions** in data distributions that are sensitive to possible SUSY signals and looking whether there is a significant excess over the SM background predictions in these regions. This also includes looking for abnormal tails in distributions of different variables that are not in agreement with the SM predictions. These variables will be discussed in the subsection 3.4.1. Signal regions are usually determined using the “cut-and-count” approach that will be discussed in the subsection 3.5.

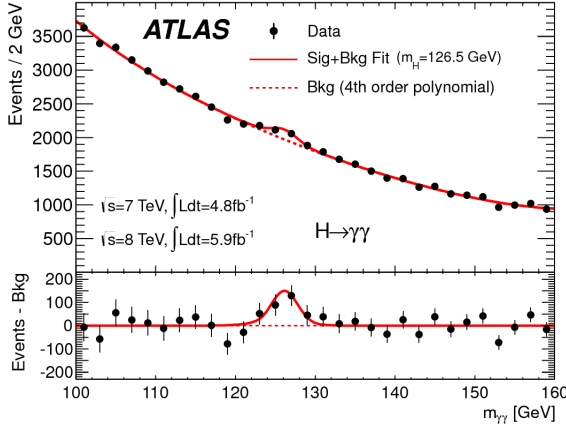


Figure 3.5: Invariant mass distribution of diphoton candidates for the combined  $\sqrt{s} = 7$  TeV and  $\sqrt{s} = 8$  TeV data samples. The mass of the Higgs corresponds to the peak at 126.5 GeV [1].

### 3.3 Overview of background processes

In order to distinguish new physics events from the SM events it is necessary to be able to suppress all SM events that have the same final state. Within the scope of this thesis that includes events that have precisely two leptons with opposite charge. The processes described in this section constitute MC simulated background that was used in the search for signal regions.

The  $Z$ +jets background comes from the production of jets of particles in association with a  $Z$  boson or a virtual photon (Drell-Yan process), which then decays into two leptons.  $t\bar{t}$  pair creation is a common process in  $pp$  collisions and is one of the dominant processes in dilepton decays. The quark-antiquark pair decays via the  $W^+bW^-\bar{b}$  intermediate state into three different final states with either no leptons, one lepton, or two leptons (here leptons include the tau). The latter decay cascade is  $t\bar{t} \rightarrow W^+bW^-\bar{b} \rightarrow \ell\nu\ell\nu b\bar{b}$ . Final states that include electrons and muons constitute around 5% of the entire  $t\bar{t}$  production [26]. Thus, the  $t\bar{t}$  production is one of the main background processes in searches for BSM events in various channels, not only those involving two-lepton final states.

The diboson production channel is dominated by the production of the  $WW$  pair with subsequent decay into two lepton/neutrino pairs. Contributions also come from the  $ZV$  channel, where  $V = W$  or  $Z$ . Other sources of dilepton final states are  $W$ +jets and single-top quark production processes. Both of them have a decay channel with final states containing a lepton and a neutrino, however their overall contribution to the background is small compared to diboson,  $t\bar{t}$ , and  $Z$ +jets. All the MC background

predictions used in this thesis belong to one of the categories described in this section.

A serious hindrance in LHC analyses is the phenomenon of “pileup”. Among the collisions that produce events of interest there are additional collisions that contaminate the output with extra jets. Along with this, tighter spacing between bunches means that for a specific collision, additional jets might originate from a neighbouring collision as the sensitivity windows for many ATLAS subsystems are longer than 25 ns [27]. Dealing with the increased pileup presents an additional challenge at the  $\sqrt{s} = 13$  TeV run, because of additional jet contamination of the data.

### 3.4 Event selection and $b$ -tagging

Event reconstruction is the process of turning raw data into manageable format that includes quantities needed in physics analysis. An event has to pass certain identification criteria to be chosen for reconstruction. Correct identification of different physics objects at LHC includes a large number of dedicated algorithms which are not presented in this thesis, but are available elsewhere [28]. However, in this section a very general outline of the selection procedure for reactions that result in two leptonic decays will be given. All “signal” objects have to pass a set of criteria to obtain a high quality sample with minimum possible contamination.

Signal electrons are required to have  $|\eta| < 2.47$  and transverse momentum  $p_T > 10$  GeV. These are inferred from the calibrated energy deposits in the EmCal and must have a matching ID track. Signal muons are reconstructed using information from MS and ID tracks and are required to have  $|\eta| < 2.5$  and  $p_T > 10$  GeV. Jets are reconstructed using information from calorimeters and are divided into “central” and “forward” categories. Central jets must have  $|\eta| < 2.4$  and  $p_T > 20$  GeV. Forward jets are those with  $2.4 < |\eta| < 4.5$  and  $p_T > 30$  GeV.

One of the common techniques used in LHC analyses is the identification of central jets that have  $b$ -hadrons (hadrons containing bottom quark/s). These jets are referred to as  $b$ -tagged and are identified using multivariate techniques based on machine learning instruments such as artificial neural networks and boosted decision trees [29]. The efficiency of  $b$ -tagging has been significantly improved in run-II due to the addition of the Insertable B-Layer in the ID.  $b$ -tagging is an extremely useful technique because some important heavy particles such as top quark and the Higgs decay into bottom quarks.

### 3.4.1 Event variables used in the analysis

A set of discriminating variables associated with searches for evidence of SUSY is presented here. Topological and kinematic variables as well as quantities derived from them will be investigated.

$\mathbf{p}_T^X$  The transverse momentum of an object  $X$ .

$\Delta\phi(X, Y)$  The difference in the azimuthal angle between two reconstructed objects  $X$  and  $Y$ , e.g.  $\Delta\phi(E_T^{miss}, \ell)$ .

$E_T^{miss}$  The magnitude of the missing transverse momentum of the event. Missing transverse momentum is defined as the negative vector sum of the transverse momenta of all identified objects.

$E_T^{miss,rel}$  This value is defined as

$$E_T^{miss,rel} = \begin{cases} E_T^{miss} & \text{if } \Delta\phi(E_T^{miss}, \ell/j) \geq \pi/2, \\ E_T^{miss} \times \sin\Delta\phi(E_T^{miss}, \ell/j) & \text{if } \Delta\phi(E_T^{miss}, \ell/j) < \pi/2 \end{cases}$$

where  $\Delta\phi(E_T^{miss}, \ell/j)$  is the azimuthal angle between the direction of  $E_T^{miss,rel}$  and that of the nearest electron, muon, or central jet.

$\mathbf{p}_{T,\ell\ell}$  The transverse momentum of the two-lepton system.

$m_{\ell\ell}$  The invariant mass of the two leptons.

Another derived event variable is the so-called “stransverse mass”  $m_{T2}$  which was introduced as a way to infer information about undetected particles [30, 31]. Along with that, it is also proved useful in suppressing backgrounds. It is used to bound the masses of a pair of supersymmetric particles each of them decaying into one visible and one invisible particle. It is a function of the momenta of two visible particles and the missing transverse momentum of an event. Its abbreviated mathematical description is as follows

$$m_{T2} = \min_{\mathbf{q}_T} \left[ \max \left( m_T(\mathbf{p}_T^{\ell 1}, \mathbf{q}_T), m_T(\mathbf{p}_T^{\ell 2}, \mathbf{p}_T^{miss} - \mathbf{q}_T) \right) \right], \quad (3.1)$$

where  $\mathbf{p}_T^{\ell 1}$  and  $\mathbf{p}_T^{\ell 2}$  are the transverse momenta of the two leptons, and  $\mathbf{q}_T$  is a transverse vector that minimizes the larger of two transverse masses  $m_T$  which is defined as

$$m_T(\mathbf{p}_T, \mathbf{q}_T) = \sqrt{2(p_T q_T - \mathbf{p}_T \cdot \mathbf{q}_T)}. \quad (3.2)$$

The  $m_{T2}$  has an upper end at the  $W$  mass for SM  $t\bar{t}$  and  $WW$  events, where the missing momentum originates from neutrinos. In case with signal events, where the LSP contributes to  $\mathbf{p}_T^{\text{miss}}$ , the  $m_{T2}$  endpoint is correlated to the mass difference between the chargino and the lightest neutralino.  $m_{T2}$  is more sensitive to large mass splittings as its distribution then extends significantly beyond the distributions of  $t\bar{t}$  and  $WW$  events. Its performance decreases for signals with small mass splittings.

### 3.5 Cut-and-count approach and test statistics

As discussed previously, a good signal region retains as many signal events as possible while at the same time cutting off background events. The way to suppress the background is to use successive cuts. The cuts are based on determining physical quantities that are able to discriminate between signal and background. The choice for a single cut is motivated both by theoretical considerations and the shapes of the MC signal and background distributions.

To optimize a cut or a set of cuts a metric that shows their discriminating power is needed. The numerical expression of how well a cut performs is given by a score function and its result will be referred to as “significance”. The score function is constructed in the following way. The total number of events in a particular selection is  $N$ , and it is the sum of  $S$  and  $B$ . The latter two refer to the number of signal and background events respectively. This gives the following expression

$$S = N - B \quad (3.3)$$

The uncertainty of  $S$  is then

$$\sigma^2(S) = \sigma^2(N) + \sigma^2(B) = N + \sigma^2(B). \quad (3.4)$$

$N$  is a mean value of a distribution described by Poisson statistics where the uncertainty is  $\sigma = \sqrt{\lambda}$ , so squaring it back just yields  $N$ .  $\sigma(B)$  is the uncertainty on the estimated average of the  $B$  value. Because estimation of the background is done with large MC statistics the  $\sigma(B)$  in this case can be treated as negligible. So what is left is

$$\frac{S}{\sigma(S)} = \frac{S}{\sqrt{N}} = \frac{S}{\sqrt{S+B}}. \quad (3.5)$$

This determines the number of standard deviations away from the 0 of the signal. Due to SUSY signals being very small compared to the background, further simplification

can be done, so that the above expression becomes

$$\frac{S}{\sigma(S)} \simeq \frac{S}{\sqrt{B}}. \quad (3.6)$$

The process of scientific discovery relies predominantly on using statistical methods to justify new discoveries and safeguard against false ones. It is especially important in HEP as it operates on quantum level where almost everything is described using probabilistic arguments (a particle’s wave function being the most obvious example).

Any potential discovery in HEP must comply with stringent requirements posed by statistical inference. If some signal has a mean that is away from the mean of the background-only sample by three standard deviations ( $3\sigma$ ), it is referred to as “evidence”. If it is a  $5\sigma$  event then it is claimed as a discovery. To put this into perspective, the chance of a  $5\sigma$  event being just random fluctuation is around 1 in 3.5 million. The expression  $S/\sqrt{B}$  thus is a rough estimate of the number of standard deviations and can serve as a metric to assess the quality of candidate signal regions.

### 3.6 Computational tools

Most of the HEP analyses are performed with ROOT framework which was developed at CERN specifically for this purpose [32]. It is a multi-purpose package that provides tools for big data processing, statistical analysis, visualisation and storage. It is written in C++ programming language, but also provides integration with other languages such as Python, Ruby, R, etc. ROOT is especially convenient because it provides constructors and methods created specifically for the LHC geometry and the type of analyses it entails. All the computational manipulations and visualisations were performed in ROOT using applications written in C++ and Python.

## CHAPTER IV

# Determining signal regions

### 4.1 First view

A common practice in SUSY dilepton analyses is to divide events into same flavour (SF) and different flavour (DF) varieties. SF thus includes events with pairs of only electrons or only muons in their final states, and DF refers to the events that decay into an electron-muon pair. In this analysis this convention will be followed.

The preliminary cuts on the pair of electrons were  $\mathbf{p}_{\mathrm{T},e_1} > 25 \text{ GeV}$  and  $\mathbf{p}_{\mathrm{T},e_2} > 20 \text{ GeV}$ , where  $e_1$  refers to the leading lepton with the largest momentum and  $e_2$  to the second one. For a muon pair the following requirements were imposed: leading muon  $\mathbf{p}_{\mathrm{T},\mu_1} > 25 \text{ GeV}$ , second muon  $\mathbf{p}_{\mathrm{T},\mu_2} > 10 \text{ GeV}$ , and the invariant mass  $m_{\mu\mu} > 20 \text{ GeV}$ . These cuts were motivated by the trigger efficiency for offline lepton candidates' identification (see Fig. A.1 and A.2 in the appendix A).

First, histograms showing the entirety of the 2015 data, MC background and signal simulations were plotted. Fig. 4.1a shows the distribution of the  $m_{\ell\ell}$  in the SF channel. The largest background contributions come from  $Z+\text{jets}$ , diboson, and  $t\bar{t}$  processes. The pronounced peak in the SF dilepton invariant mass distribution is in the 80-100 GeV bin due to the contribution from the  $Z+\text{jets}$  component. This background can be suppressed by introducing  $m_Z$ -veto which cuts out all events within 10 GeV from the mass of the  $Z$  boson (91.2 GeV). However, after this cut, the distribution will still retain events from the off mass-shell decays of the  $Z$  boson.

The histogram for DF channel (Fig. 4.1b) shows that there is a much smaller contribution from  $Z+\text{jets}$  component in this channel compared to the SF one. Thus  $m_Z$  veto here can be avoided. The diboson and  $t\bar{t}$  processes, however, prevail in this channel as well.

The dotted lines are the shapes of signal distributions and they are in accordance with the mass of the chargino pair. The blue line represents 200-150 mass splitting,

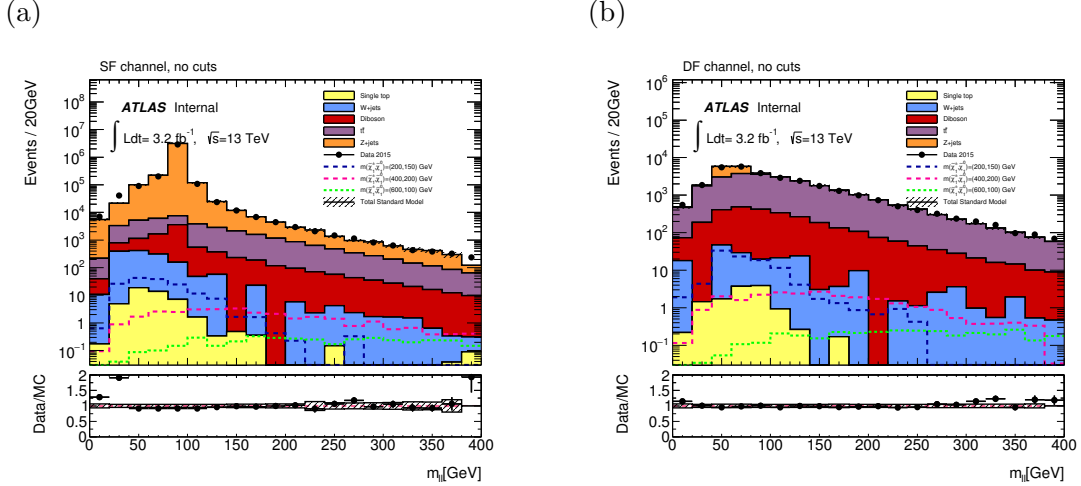


Figure 4.1: Dilepton invariant mass distributions for SF and DF channels.

so its events are concentrated in the lower mass regions. The pink and green lines represent 400-200 and 600-100 signals respectively, and also are distributed according to this logic.

## 4.2 Cuts in the SF channel

As was mentioned in the previous section the the following veto was imposed on all the signal regions in SF channel:

$$|m_{\ell\ell} - m_Z| > 10 \text{ GeV} \text{ (with } m_Z = 91.2 \text{ GeV)}$$

The next step was to veto all the jets to reduce  $t\bar{t}$  contribution. The result of this combination of vetoes can be seen in Fig. 4.2. As expected the  $m_{T2}$  distribution is dependent on the mass splitting and is better for 400-200 and 600-100 signals. At this point it is possible to calculate sensitivity values by placing cuts on  $m_{T2}$  and the results can be seen in Tab. 4.1. No signal was obtained for 200-150 signal, therefore it is omitted from the table. The best result was the projected significance of 3.62 at  $19.2 \text{ fb}^{-1}$  with  $m_{T2} > 100 \text{ GeV}$  cut.

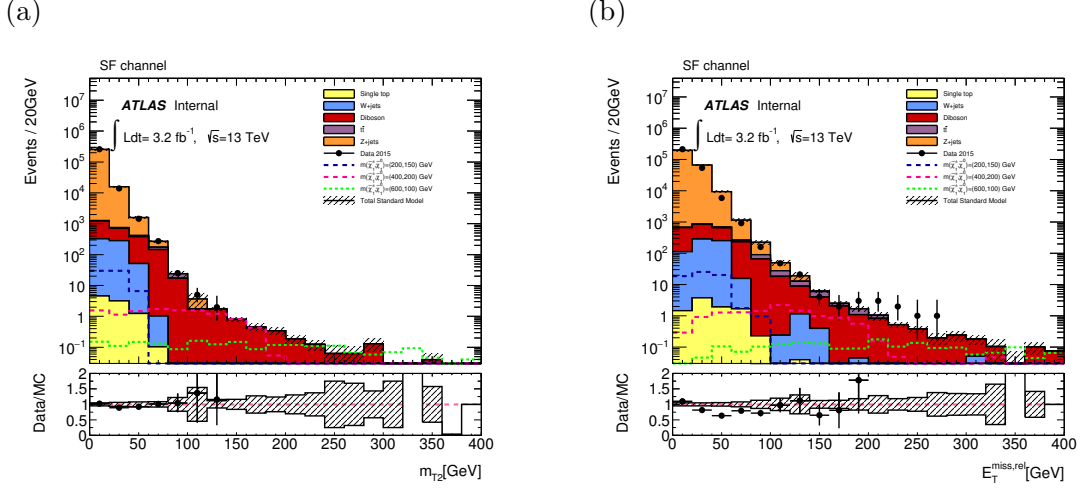


Figure 4.2: The  $E_T^{\text{miss,rel}}$  and  $m_{T2}$  distributions for SF channel, with cuts on  $m_Z$  and no jets.

$\int \mathcal{L} dt$	3.2 $\text{fb}^{-1}$		9.6 $\text{fb}^{-1}$		19.2 $\text{fb}^{-1}$	
Signal models	<b>400-200</b>	<b>600-100</b>	<b>400-200</b>	<b>600-100</b>	<b>400-200</b>	<b>600-100</b>
$m_{T2} > 80 \text{ GeV}$	1.01	0.26	1.74	0.45	2.46	0.64
$m_{T2} > 100 \text{ GeV}$	1.47	0.50	2.56	0.86	3.62	1.22
$m_{T2} > 120 \text{ GeV}$	1.27	0.61	2.19	1.06	3.09	1.5

Table 4.1: Significance values ( $S/\sqrt{B}$ ) for the SF channel signal models with various cuts on  $m_{T2}$  at increasing integrated luminosities. For all signals cuts are placed on  $m_Z$  and no jets are allowed.

## **APPENDICES**

## APPENDIX A

### Trigger Efficiencies

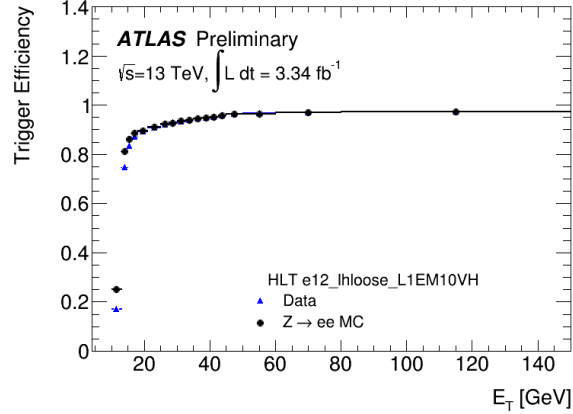


Figure A.1: Electron trigger efficiency as a function of the offline electron candidates  $E_T$  [33].

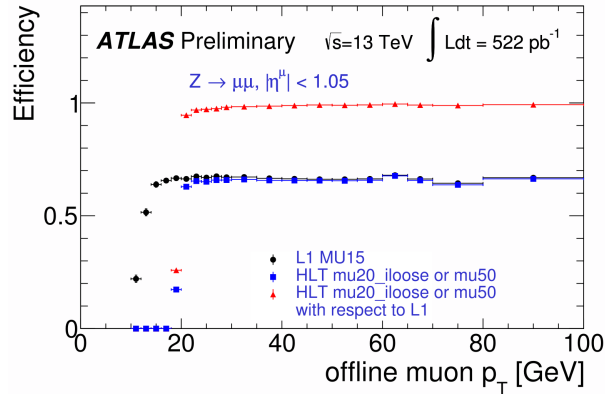


Figure A.2: Muon trigger efficiency as a function of  $p_T$  of offline muon candidates [34].

# Bibliography

- [1] G. Aad *et al.*, “Observation of a new particle in the search for the Standard Model Higgs boson with the ATLAS detector at the LHC,” *Phys. Lett.*, vol. B716, pp. 1–29, 2012.
- [2] S. Chatrchyan, V. Khachatryan, A. M. Sirunyan, A. Tumasyan, W. Adam, E. Aguilo, T. Bergauer, M. Dragicevic, J. Erö, C. Fabjan, *et al.*, “Observation of a new boson at a mass of 125 gev with the cms experiment at the lhc,” *Physics Letters B*, vol. 716, no. 1, pp. 30–61, 2012.
- [3] B. R. Martin, *Nuclear and particle physics: An introduction*. John Wiley & Sons, 2006.
- [4] S. L. Glashow, “Partial Symmetries of Weak Interactions,” *Nucl. Phys.*, vol. 22, pp. 579–588, 1961.
- [5] S. Weinberg, “A model of leptons,” *Physical review letters*, vol. 19, no. 21, p. 1264, 1967.
- [6] A. Salam and N. Svartholm, “Elementary particle theory,” *Almqvist and Wiksell, Stockholm*, p. 367, 1968.
- [7] F. Englert and R. Brout, “Broken symmetry and the mass of gauge vector mesons,” *Physical Review Letters*, vol. 13, no. 9, p. 321, 1964.
- [8] P. W. Higgs, “Broken symmetries and the masses of gauge bosons,” *Physical Review Letters*, vol. 13, no. 16, p. 508, 1964.
- [9] E. Gildener, “Gauge-symmetry hierarchies,” *Phys. Rev. D*, vol. 14, pp. 1667–1672, Sep 1976.
- [10] P. A. Ade, N. Aghanim, M. Alves, C. Armitage-Caplan, M. Arnaud, M. Ashdown, F. Atrio-Barandela, J. Aumont, H. Aussel, C. Baccigalupi, *et al.*, “Planck 2013 results. I. overview of products and scientific results,” *Astronomy & Astrophysics*, vol. 571, p. A1, 2014.
- [11] CMS , “Are there more particles left to find? supersymmetry: uniting the forces,” 2011. [Online; accessed May 18, 2016].

- [12] J. D. Lykken, “Introduction to supersymmetry,” in *Fields, strings and duality. Proceedings, Summer School, Theoretical Advanced Study Institute in Elementary Particle Physics, TASI’96, Boulder, USA, June 2-28, 1996*, pp. 85–153, 1996.
- [13] G. Aad, E. Abat, J. Abdallah, A. Abdelalim, A. Abdesselam, O. Abdinov, B. Abi, M. Abolins, H. Abramowicz, E. Acerbi, *et al.*, “The atlas experiment at the cern large hadron collider,” *Journal of Instrumentation*, vol. 3, no. 8, 2008.
- [14] G. Aad, B. Abbott, J. Abdallah, A. Abdelalim, A. Abdesselam, O. Abdinov, B. Abi, M. Abolins, H. Abramowicz, H. Abreu, *et al.*, “The atlas inner detector commissioning and calibration,” *The European Physical Journal C*, vol. 70, no. 3, pp. 787–821, 2010.
- [15] Pequenao, Joao, “Event cross section in a computer generated image of the atlas detector.,” 2008. [Online; accessed May 18, 2016].
- [16] G. Aad, B. Abbott, J. Abdallah, A. Abdelalim, A. Abdesselam, O. Abdinov, B. Abi, M. Abolins, H. Abramowicz, H. Abreu, *et al.*, “Performance of the atlas trigger system in 2010,” *The European Physical Journal C*, vol. 72, no. 1, pp. 1–61, 2012.
- [17] G. Barr, R. Devenish, R. Walczak, and T. Weidberg, *Particle Physics in the LHC Era*. Oxford University Press, 2015.
- [18] C. Borschensky, M. Krämer, A. Kulesza, M. Mangano, S. Padhi, T. Plehn, and X. Portell, “Squark and gluino production cross sections in pp collisions at  $\sqrt{s}=13, 14, 33$  and 100 tev,” *The European Physical Journal C*, vol. 74, no. 12, pp. 1–12, 2014.
- [19] G. Aad, B. Abbott, J. Abdallah, O. Abdinov, R. Aben, M. Abolins, O. AbouZeid, H. Abramowicz, H. Abreu, R. Abreu, *et al.*, “Summary of the searches for squarks and gluinos using  $\sqrt{s} = 8$  tev pp collisions with the atlas experiment at the lhc,” *Journal of High Energy Physics*, vol. 2015, no. 10, pp. 1–100, 2015.
- [20] G. Aad *et al.*, “Search for the electroweak production of supersymmetric particles in  $\sqrt{s}=8$  TeV pp collisions with the ATLAS detector,” *Phys. Rev.*, vol. D93, no. 5, p. 052002, 2016.
- [21] ATLAS collaboration, “Mass reach of atlas searches for supersymmetry,” 2016.
- [22] G. Aad, B. Abbott, J. Abdallah, O. Abdinov, R. Aben, M. Abolins, O. AbouZeid, H. Abramowicz, H. Abreu, R. Abreu, *et al.*, “Search for the electroweak production of supersymmetric particles in  $s=8$  tev p p collisions with the atlas detector,” *Physical review D*, vol. 93, no. 5, p. 052002, 2016.
- [23] B. Fuks, M. Klasen, D. R. Lamprea, and M. Rothering, “Gaugino production in proton-proton collisions at a center-of-mass energy of 8 TeV,” *JHEP*, vol. 10, p. 081, 2012.

- [24] B. Fuks, M. Klasen, D. R. Lamprea, and M. Rothering, “Precision predictions for electroweak superpartner production at hadron colliders with RESUMMINO,” *Eur. Phys. J. C*, vol. 73, p. 2480, 2013.
- [25] ATLAS Collaboration, “Nlo-nll wino-like chargino-chargino (c1c1) cross sections.” <https://twiki.cern.ch/twiki/bin/view/LHCPhysics/SUSYCrossSections13TeVx1x1wino>, 2016.
- [26] W. Wagner, “Top-Antitop-Quark Production and Decay Properties at the Tevatron,” *Mod. Phys. Lett.*, vol. A25, pp. 1297–1314, 2010.
- [27] Z. Marshall, “Simulation of Pile-up in the ATLAS Experiment,” *J. Phys. Conf. Ser.*, vol. 513, p. 022024, 2014.
- [28] G. Aad *et al.*, “Search for supersymmetry at  $\sqrt{s} = 13$  TeV in final states with jets and two same-sign leptons or three leptons with the ATLAS detector,” *Eur. Phys. J.*, vol. C76, no. 5, p. 259, 2016.
- [29] G. Aad *et al.*, “Performance of  $b$ -Jet Identification in the ATLAS Experiment,” *JINST*, vol. 11, no. 04, p. P04008, 2016.
- [30] C. G. Lester and D. J. Summers, “Measuring masses of semiinvisibly decaying particles pair produced at hadron colliders,” *Phys. Lett.*, vol. B463, pp. 99–103, 1999.
- [31] A. Barr, C. Lester, and P. Stephens, “ $m(T2)$ : The Truth behind the glamour,” *J. Phys.*, vol. G29, pp. 2343–2363, 2003.
- [32] “ROOT Data Analysis Framework.” <https://root.cern.ch/>.
- [33] ATLAS Collaboration, “Electron trigger performance in 2015 ATLAS data (December 6, 2015) .” [https://twiki.cern.ch/twiki/bin/view/AtlasPublic/EgammaTriggerPublicResults#Electron\\_trigger\\_performance\\_AN2](https://twiki.cern.ch/twiki/bin/view/AtlasPublic/EgammaTriggerPublicResults#Electron_trigger_performance_AN2).
- [34] ATLAS Collaboration, “Muon trigger performances in 2015 25ns data-taking period.” [https://twiki.cern.ch/twiki/bin/view/AtlasPublic/MuonTriggerPublicResults#Muon\\_trigger.Performances\\_in\\_2015](https://twiki.cern.ch/twiki/bin/view/AtlasPublic/MuonTriggerPublicResults#Muon_trigger.Performances_in_2015).